Energy Storage and Conversion 2024, 2(2), 1151.
https://doi.org/10.59400/esc.v2i2.1151.

Article

AlZnO magnetron sputtered thin film for photovoltaic application

Zohreh Ghorannevis[1,*], Mehran Jamalpourkolour[1], Arash Boochani[2], Arash Yari[2], Nosratali Vahabzadeh[3], Parnia Goudarzi[4]

[1] Department of Physics, Karaj Branch, Islamic Azad University, Alborz, Iran
[2] Department of Physics, Kermanshah Branch, Islamic Azad University, Kermanshah, Iran
[3] Department of Physics, Parsabad Moghan Branch, Islamic Azad University, Parsabad Moghan, Iran
[4] Plasma Physics Research Center, Science and Research Branch, Islamic Azad University, Tehran, Iran
*** Corresponding author:** Zohreh Ghorannevis, ghoranneviszohreh@gmail.com

CITATION

Ghorannevis Z, Jamalpourkolour M, Boochani A, et al. AlZnO magnetron sputtered thin film for photovoltaic application. 2024; 2(2): 1151. https://doi.org/10.59400/esc.v2i2.1151

ARTICLE INFO

Received: 5 March 2024
Accepted: 26 April 2024
Available online: 16 May 2024

Abstract: Aluminum zinc oxide (AZO) is a nontoxic and low-cost material that finds application as a transparent conducting electrode in photovoltaic devices. In this study, the (direct current) DC magnetron sputtering of AZO films is carried out at different deposition times of 5, 10, 15, 20, and 25 min's at room temperature, and its structural, optical, electrical, and morphological properties are studied for its use as a front contact for thin film solar cell application. The structural study suggests that the preferred orientation of grains along the (002) plane has a hexagonal structure, and the optical and electrical studies suggest that the films show an average transmission of 70% and a resistivity of the order of $10^{-4}\Omega$ cm. On the other hand, the scanning electron microscopy (SEM) images suggest the formation of packed grains with a homogeneous surface. Moreover, in order to study the optoelectronic properties of prepared samples, the electronic and optical calculations of the AZO are performed by the first-principles calculations using density functional theory (DFT).

Keywords: AZO; sputtering; photovoltaic; thin film solar cell; DFT

1. Introduction

Aluminum zinc oxide (AZO) is a transparent conducting oxide (TCO) material owing to its nontoxicity as well as its tunable optoelectronic properties [1–5]. AZO thin films are widely used in photonic devices such as light-emitting diodes (LED's) [6], thin film solar cells [7,8], flat panel displays [9], as well as sensing devices [10,11]. It is notable that the above applications require conductivity (sheet resistance <10 ohms per square) as well as high transmittance (>80%) in the visible region. There are different techniques to prepare AZO films, such as sputtering [12], electron beam evaporation [13], pulsed laser deposition [14], chemical vapor deposition [15], spray pyrolysis [16], and sol-gel deposition [17], that are well reported for preparing AZO thin films on different substrates. Direct current (DC) magnetron sputtering is an industrially acceptable technique due to its convenience, high deposition rate, and scalability over a large area [18]. Generally speaking, the most commonly preferred substrate of all TCO films is glass, and the physics properties of sputtered AZO thin films are highly sensitive to controlled process parameters such as base vacuum, gas pressure, substrate temperature, and deposition time. Therefore, in this study, optimized experimental conditions are found to investigate the effect of deposition time on the physical properties of AZO thin film deposited on soda lime glass substrate. The effect of deposition time is estimated on the structural, optical, morphological, and electrical properties in order to achieve the lowest resistivity and

the highest transparency for the films. On the other hand, the electronic and optical calculations of the AZO films are also performed by first-principles calculations using DFT in order to achieve more detailed studies on the prepared AZO thin film.

2. Materials and methods

Figure 1 shows a schematic diagram of a magnetron sputtering system that is used in these experiments. AZO thin films are deposited using a magnetron sputtering setup on a 3-inch-diameter target consisting of 98 wt% ZnO and 2 wt% Al_2O_3. It is worth nothing that the films are deposited at room temperature, and no oxygen is introduced in this process. First of all, the glass substrates are ultrasonically cleaned in sequentially distilled water, acetone, alcohol, distilled water, and finally dried with nitrogen gas. The substrates are then placed at a distance of a distance of 70 mm from the target. The sputtering chamber is first pumped to a base vacuum pressure of 10^{-6} Torr, and the Ar gas is introduced into the chamber. The sputtering gas pressure is set to be about 2×10^{-2} Torr. After the deposition, the samples are self-cooled and later examined for their physical properties. The surface morphology of the films and the crystal structure are studied using a field-effect scanning electron microscope (FESEM) and an X-ray diffractometer (XRD), respectively. A Dektak profilometer is also used to estimate the film thicknesses. The optical transmission measurements are also carried out with a spectrophotometer in the spectral region of 190–800 nm, and the atomic force microscope (AFM) images are also taken under the contact mode to evaluate the roughness of the films. Moreover, the resistivities of the films are measured using a four-point probe method.

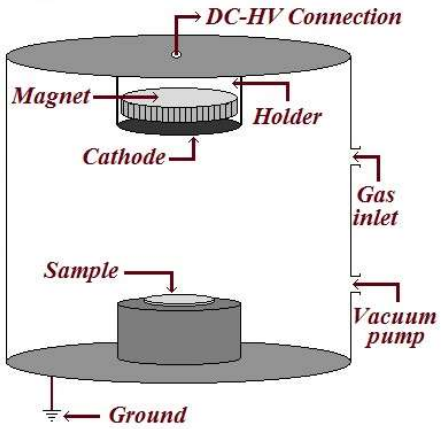

Figure 1. Schematic of magnetron sputtering setup.

3. Results

3.1. Experimental

AZO thin films prepared at different deposition times while keeping other experimental conditions constant are studied for their physical properties. By increasing the deposition time, the film thicknesses are also increased. **Table 1** gives the thicknesses of the AZO thin films prepared at different deposition times of 5, 10, 15, 20, and 25 min.

Table 1. Thicknesses of the AZO thin films prepared at different deposition times.

Thickness	Deposition time
210 nm	5 min
350 nm	10 min
520 nm	15 min
710 nm	20 min
1150 nm	25 min

Figure 2a shows the XRD spectra of AZO films grown at different deposition times. The XRD data's 5 min is not enough time to form the film, and the XRD data does not show any AZO peak. However, the film grown at the deposition time of 20 min shows a (002) peak with high intensity, which becomes much stronger, sharper, and narrower. A small diffraction intensity from (004) planes also appears in the XRD spectra. As it can be seen from **Figure 2b,** the (004) peak intensity is very low in comparison with the (002) peak intensity. Both peaks belong to AZO structures with two different planes. Moreover, a higher XRD intensity corresponds to improved film crystallinity for 20 min. It is clear that all the polycrystalline AZO thin films deposited on the glass substrates exhibit (002) crystallographic orientation due to the minimal surface energy in the ZnO hexagonal wurtzite structure. The appearance of a (002) peak in this spectra indicates that the films grown at different deposition times have a c-axis preferred orientation due to a self-texturing phenomenon [16].

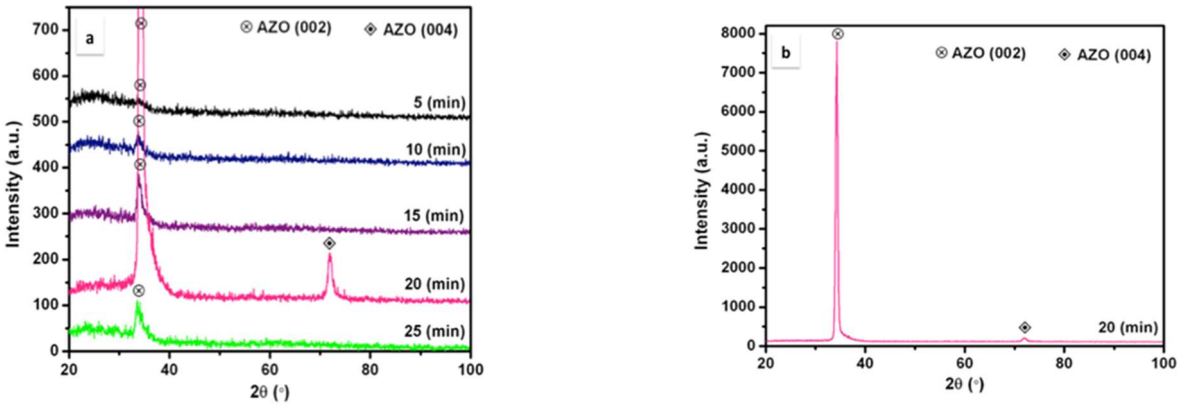

Figure 2. XRD spectra of AZO films deposited at **(a)** various deposition times; **(b)** 20 min.

From the XRD spectrum, the crystalline quality of the AZO thin films becomes weak for the higher deposition times (25 min), and no peaks corresponding to the Al_2O_3 phase are seen in the XRD pattern, which may be due to the aluminum replacing zinc substitutionally in the hexagonal lattice. From the XRD data, the average grain size of the AZO thin film can also be evaluated by the Debye-Scherrer equation [16] as follows:

$$\text{Grain size} = 0.9\,\lambda/\beta\cos\theta \quad (1)$$

where λ is the X-ray wavelength (0.154 nm), θ is the Bragg angle, and β is the full width at half maximum (FWHM) of the diffraction peak. The calculated crystal sizes of the thin films are more or less uniform for all the films, ranging from 8 to 19 nm

(**Table 2**). The maximum grain size is around 19.231 nm for the sample prepared at the 20 min deposition time.

Table 2. Calculated grain sizes and FWHM for AZO films grown at different deposition times for (002) peaks.

Time (min)	D-spacing (Å)	FWHM (degree)	Grain size (nm)
5	2.659	0.59	14.483
10	2.656	0.96	8.725
15	2.654	0.72	11.680
20	2.618	0.44	19.231
25	2.673	0.6	14.053

Figure 3 shows the graph of the FWHM of (002) and (004) XRD peaks and the corresponding grain sizes of the AZO thin films as a function of crystal planes. It is observable that the grain size for the (004) peak is larger, and the average grain size for both AZO crystal planes is around 20 nm.

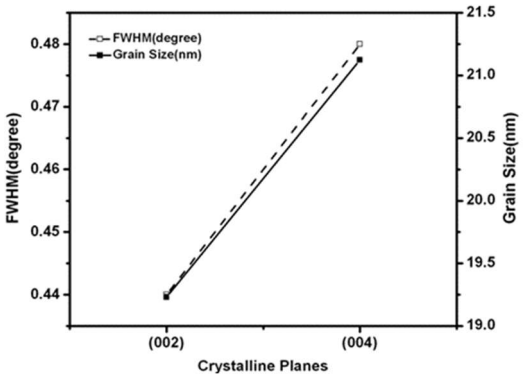

Figure 3. FWHM and grain size of (002) and (004) XRD peaks corresponding to the AZO thin film as a function of crystal planes.

Figure 4 shows the optical transmittance of the AZO thin films measured by a UV-VIS spectrophotometer in the frequency range of 200–800 nm. All the thin films sputtered at the different deposition times exhibit more than 70% transmittance in the visible region.

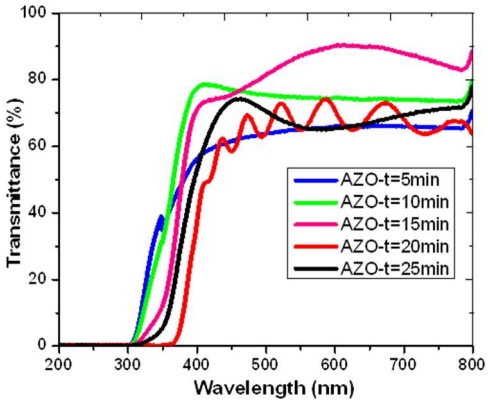

Figure 4. The transmission over the VIS range for AZO thin film at different deposition times.

An excellent surface quality and homogeneity of the film are confirmed by the appearance of interference fringes in the transmission spectra occurring when the film surface is reflecting without much scattering/absorption in the bulk of the film [17]. As can be seen in **Figure 5,** the film, which was prepared at 20 min shows these interference fringes. The electrical resistivity of the films is also given in **Table 3** for the different deposition times of the prepared samples. The lowest resistivity of the films is measured to be 4.1×10^{-4}. It can be seen that the resistivity increases as the deposition time increases to 20 min and then decreases as the deposition time increases to 25 min. Increasing the crystallite size of AZO thin films can decrease the grain boundary scattering and increase the carrier lifetime to achieve the lower resistivity of the AZO thin films.

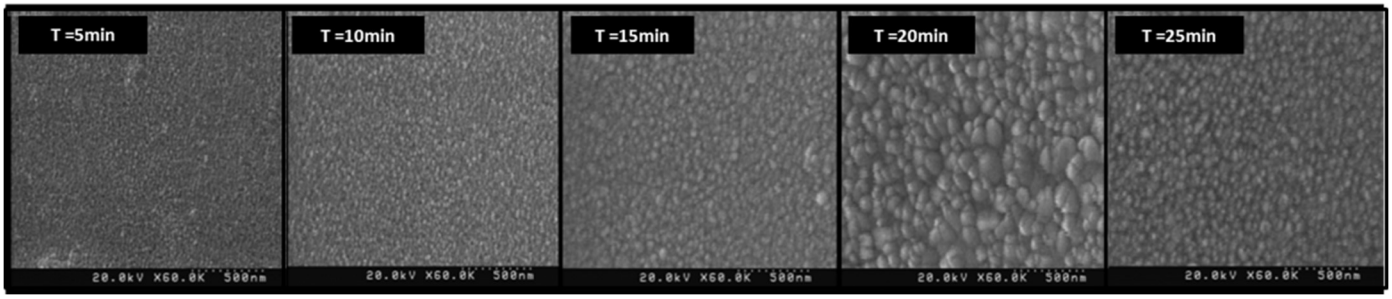

Figure 5. SEM images of AZO thin films at different deposition times.

Table 3. Electrical resistivities measured for the AZO thin films prepared at different deposition times.

Resistivity (Ωcm)	**Deposition time**
9.8×10^{-2}	5 min
3.6×10^{-2}	10 min
3.2×10^{-3}	15 min
4.1×10^{-4}	20 min
1.2×10^{-3}	25 min

SEM images of AZO are shown in **Figure 5**. These images can be used to study the AZO film surface morphology and microstructure, which show the surface micrographs of the films as a function of the deposition time. It is found that the deposition time has a great influence on the film surface structure. The AZO film deposited at 20 min shows surface features of densely packed grains and the grains that are aggregating.

Moreover, AFM images are given in **Figure 6** for the AZO thin films deposited at different deposition times. It is known that surface roughness is one of the important factors in the AZO thin film for many optoelectronic applications because the level of surface roughness will dominate carrier mobility and light scattering [19,20]. In **Figure 6**, the rough and non-uniform surface structures of the AZO thin films at the different deposition times are observed. The roughness of the films is given in **Table 4**. As it can be seen, the roughness is increased by increasing the deposition time to 20 min due to the density of the thin film, which is enhanced by increasing the deposition time.

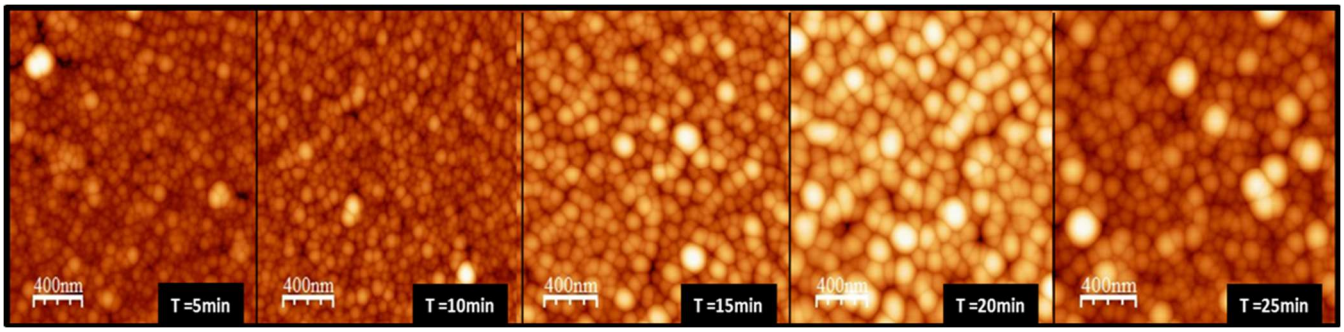

Figure 6. AFM images of AZO thin films deposited at different deposition times.

Table 4. Average roughnesses of the AZO thin films deposited at different deposition times.

Roughness	Deposition time
28.4 nm	5 min
33.4 nm	10 min
48.7 nm	15 min
49.3 nm	20 min
38.4 nm	25 min

3.2. Computational

The electronic and optical calculations of the AZO film are performed by first-principles calculations using density functional theory (DFT) [21–23]. Solving the Kohn-Sham equations is done using the full potential method of linear augmented waves (FP-LAPW) [24], which is used in the WIEN2k package [25]. The PBE-GGA approximation is used to solve the exchange-correlation potential for greater accuracy [26]. The optimized input parameters, including RKmax, KPoint, lmax, and separation energy, are selected as 8.0, 10 × 10 × 2, 10 and –7.0 Ryd, respectively. The muffin tin values of the Zn, O, and Al atoms are selected at 2.20 a.u., 1.45 a.u., and 1.8 a.u., respectively. The force convergence of the relaxation calculations is 10^{-6} dyn/a.u., and the optical calculations are approximated by the random phase approximation (RPA) with 15 × 15 × 2KPoint in the first Brillouinzone. In **Figure 7**, panel (a), the density of electronic states (DOS) of ZnO with an Al impurity of 2% is calculated with an mBJ approximation. This diagram shows that this compound has a very weak conductivity because the electron states are partially present in the Fermi level, and in the region below the Fermi level (valence area), a 2 eV gap is seen. In the –4 eV region, there are many electron states towards the lower energies of the valence region, and also in the region of –4 eV to –9.5 eV the Van Hov singularity is observed. Therefore, during the radiation or applying the heat, there is a suitable source for excited electrons. In panel (b), the partial DOS are shown.

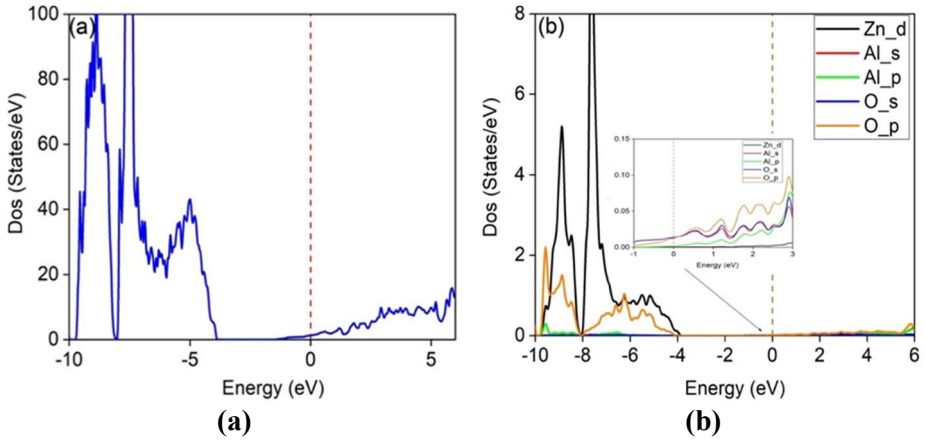

(a) **(b)**

Figure 7. (a) the density of electronic states (DOS) of ZnO with Al impurity of 2%; **(b)** the partial DOS.

It can be seen that in the valence region, the main contribution of the density of electronic states belongs to the d-Zn and p-O orbitals, and the p-O, s-O, and s-Al orbitals have the main role at the Fermi level and conduction region.

In **Figure 8**, the band structure of ZnO:Al with a 2% impurity percentage is depicted in the symmetry direction M→K→Γ→A →Γ in the first Brillouin zone. It can be seen that in the region of –9.5 eV to –4 eV, a high density of electron levels is shown, which is in perfect agreement with the DOS curves. In the region of –4.5 eV to –1.5 eV and above –1.5 eV of the Fermi level, an energy gap and electron level belonging to the s-Al orbital are given, respectively, which intersect the Fermi level. Due to the appropriate slope of this level curve, it helps the excited electrons move to the conduction region. Another point is that the gradient of the conduction region is higher than the valence region, so the excited electrons are well placed in the conduction current.

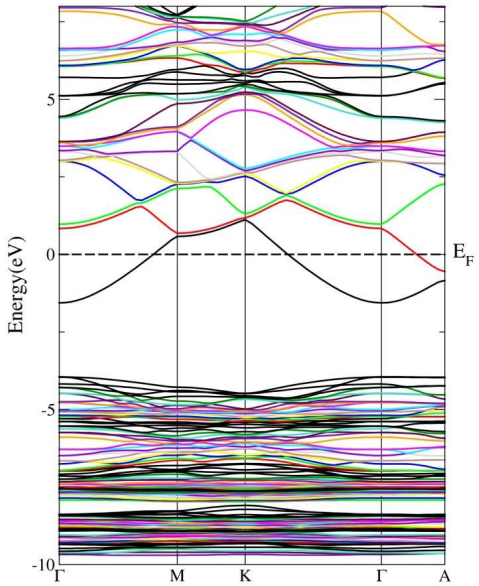

Figure 8. the band structure of AZO with 2% impurity percentage in the first Brillouin zone.

In **Figure 9**, the optical diagrams of this compound are examined. Due to the inclusion of Al impurities in the ZnO structure, its cubic symmetry is disturbed. Due to the asymmetry in the arrangement of atoms after the Al impurity atom enters the ZnO compound, the response of this compound to the light irradiated in different directions is different. Therefore, the optical behavior of the AlZnO compound was investigated in two crystal directions, x and z, which we have distinguished in the optical diagrams. Panel (a) shows the real part of the dielectric function, whose static value along the z-axis shows poor metallic behavior. However, as soon as the energy of the radiated photon increases, the dielectric function diagram is strongly reduced in Dirac form and reduced to zero and negative values, and it reaches 2.7 in the UV and visible regions. It remains constant up to the range of 8 eV.

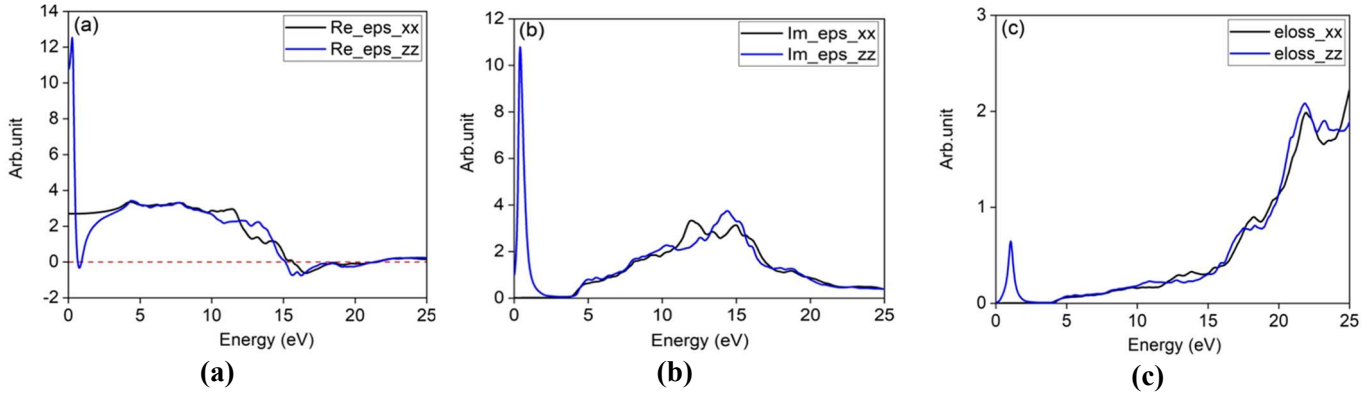

(a) **(b)** **(c)**

Figure 9. (a) real part; **(b)** imaginary part; **(c)** the spectrum of the loss of dielectric function in both x and z directions.

With radiation along the x-axis, its static value is 2.7, and it remains in this range up to 10 eV. From 10 eV onwards, this function is reduced in both directions, and at 15 eV to 20 eV, it will have negative values.The low value of the true dielectric function of this composition can be an indicator of the transparency of this composition. Panel (b) shows the imaginary part of the dielectric function in both x and z directions. Along the z-axis, we see a sharp Dirac peak that becomes zero with the increase of the emitted photon energy at the visible edge, which is consistent with the metallic behavior of this composition. Along the x-axis up to the range of 4 eV of the UV edge, a gap that increases with the increase in the energy of the irradiated photon is seen, and it has reached its maximum values from 15 to 14 eV; therefore, the electron transition occurs more at high energy. In panel (c), the spectrum of the loss function can be seen. There is a small peak in the z direction in the infrared range, which confirms the behavior of the metal. In the visible and UV ranges, the loss values are very small, and the most loss occurs in the 15 eV region. By comparing this diagram with the previous two diagrams, the transparency of this optical behavior in the infrared, visible, and UV regions is confirmed.

In **Figure 10**, the absorption, reflection coefficient, and refraction coefficient for the AZO composition are drawn. As can be seen in the absorption diagram, there is practically no absorption up to the UV edge, except for a very small peak in the direction of the z-axis, which, compared to the curves in **Figure 7**, concludes that this compound acts like a transparent material in the visible, UV, and IR regions. Also, with the increase in energy of the emitted photon, the amount of absorption increases

in both directions. In panel (b), the reflection coefficient is specified for these two directions. In the z direction, its static value is around 30%, which, of course, decreases sharply with the increase of the radiated energy and increases in the visible region. In the x direction, the value of the reflection coefficient at low energies is around 8%, and with the increase in the energy of the radiated photon, even up to the range of 15 eV, the value of the reflection coefficient for both directions is in the range of 5% to 30%, and in the IR, visible, and UV regions, it is below 10%, which again emphasizes the transparency of this composition. In panel (c), the refractive index shows that its static value is 3.2 along the z axis and 1.7 along the x axis. In the direction of the z axis, an anisotropy can be observed at low energies, which is indicative of the poor metalic behavior, but with the increase in energy of the radiated photon in both directions, the refractive index is less than 2. 10 eV and more indicates the behavior of a vacuum. It is the kind that has confirmed the transparency of the composition again.

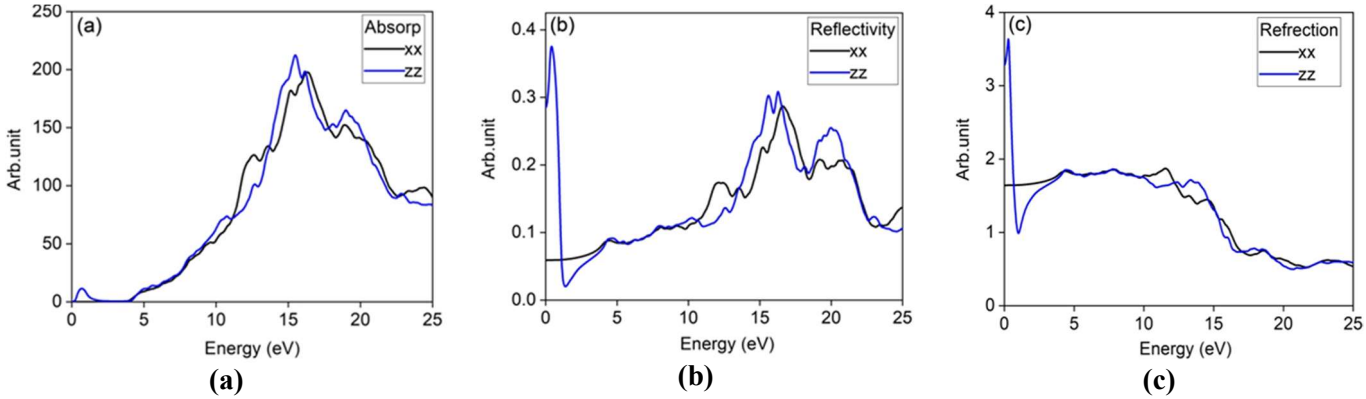

(a) **(b)** **(c)**

Figure 10. (a) absorption, **(b)** reflection coefficient, **(c)** refraction coefficient for AZO composition.

4. Discussion

AZO films are magnetron sputtered on the glass substrate at room temperature using DC magnetron sputtering to find the optimum experimental condition to make front contact for optoelectronic devices. The structural, morphological, optical, and electrical properties are studied, which suggest that the preferred orientation of grains along the (002) plane having a hexagonal structure is grown at a 20-minute deposition time that shows packed grains with a homogeneous surface. Moreover, this sample shows an average transmission of 70% and a resistivity of the order of 10^{-4} Ωcm. On the other hand, the electronic and optical calculations of the AZO are performed by first-principles calculations using density functional theory (DFT) to study more details on the physical properties of the films. DFT calculations also reveal that this compound acts like a transparent material. Therefore, experimental and theoretical results are in good agreement and confirm that the grown film has promising TCO material for optoelectronic applications.

5. Conclusion

The structural, electrical, morphological, and optical properties of AZO films deposited at room temperature on glass substrates by magnetron sputtering are

investigated to explore the possibility of producing transparent oxide films through a simple, low-cost process for photovoltaic applications. It is observed that the AZO thin films are grown with c-axis preferred orientations without degradation of the wurtzite ZnO structure. The electrical and optical properties of the AZO films improved with increasing deposition time. The higher crystallinity, lower resistivity, suitable roughness, and transmittance were obtained for the sample prepared at a 20-minute deposition time. The electronic and optical calculations of the AZO are also performed by the first-principles calculations using DFT for ZnO:Al composition with a 2% impurity percentage. This work suggests the possibility of producing AZO films with the required electrical and optical properties by a simple, low-cost process at room temperature.

Author contributions: Experimental, ZG; software, AB, AY and NV; draft ptrparation; MJ and PG. All authors have read and agreed to the published version of the manuscript.

Conflict of interest: The authors declare no conflict of interest.

References

1. Badgujar AC, Yadav BS, Jha GK, et al. Room Temperature Sputtered Aluminum-Doped ZnO Thin Film Transparent Electrode for Application in Solar Cells and for Low-Band-Gap Optoelectronic Devices. ACS Omega. 2022; 7(16): 14203-14210. doi: 10.1021/acsomega.2c00830
2. Aïssa B, Hossain MI. Photonic Cooler Based on Multistacked Thin Films with Near-Infrared Filter Properties. ACS Omega. 2024; 9(3): 3295-3304. doi: 10.1021/acsomega.3c05561
3. Pal S, Basak D. Interaction of an Ultrathin Zinc Surface Passivation Layer with a Room Temperature-Deposited Al-Doped ZnO Film Leading to Highly Improved Electrical Transport Properties. The Journal of Physical Chemistry C. 2023; 127(29): 14439–14449. doi: 10.1021/acs.jpcc.3c02329
4. Petrova D, Napoleonov B, Minh CNH, et al. The Effect of Post Deposition Treatment on Properties of ALD Al-Doped ZnO Films. Nanomaterials. 2023; 13(5): 800. doi: 10.3390/nano13050800
5. Yang B, Yao C, Yu Y, et al. Nature Degradable, Flexible, and Transparent Conductive Substrates from Green and Earth-Abundant Materials. Scientific Reports. 2017; 7, 4936. doi: 10.1038/s41598-017-04969-y
6. Chauhan RN, Tiwari N, Anand RS, et al. Development of Al-doped ZnO thin film as a transparent cathode and anode for application in transparent organic light-emitting diodes. RSC Advances. 2016; 6(90): 86770–86781. doi: 10.1039/c6ra14124b
7. Dimitrov D, Tsai CL, Petrov S, et al. Atomic Layer-Deposited Al-Doped ZnO Thin Films for Display Applications. Coatings. 2020; 10(6): 539. doi: 10.3390/coatings10060539
8. Badgujar AC, Dusane RO, Dhage SR. Cu(In,Ga)Se2 thin film solar cells produced by atmospheric selenization of spray casted nanocrystalline layers. Solar Energy. 2020; 209: 1–10. doi: 10.1016/j.solener.2020.08.080
9. Hjiri M, El Mir L, Leonardi SG, et al. Al-doped ZnO for highly sensitive CO gas sensors. Sensors and Actuators B: Chemical. 2014; 196: 413–420. doi: 10.1016/j.snb.2014.01.068
10. Yadav BS, Dey SR, Dhage SR. Effective ink-jet printing of aqueous ink for Cu (In, Ga) Se_2 thin film absorber for solar cell application. Solar Energy. 2019; 179: 363–370. doi: 10.1016/j.solener.2019.01.003
11. Samoei VK, Jayatissa AH. Aluminum doped zinc oxide (AZO)-based pressure sensor. Sensors and Actuators A: Physical. 2020; 303: 111816. doi: 10.1016/j.sna.2019.111816
12. Park KC, Ma DY, Kim KH. The physical properties of Al-doped zinc oxide films prepared by RF magnetron sputtering. Thin Solid Films. 1997; 305: 201–209. doi: 10.1016/S0040-6090(97)00215-0
13. Sahu DR, Lin SY, Huang JL. Improved properties of Al-doped ZnO film by electron beam evaporation technique. Microelectronics Journal. 2007; 38(2): 245–250. doi: 10.1016/j.mejo.2006.11.005

14. Venkatachalam S, Iida Y, Kanno Y. Preparation and characterization of Al doped ZnO thin films by PLD. Superlattices and Microstructures. 2008; 44(1): 127–135. doi: 10.1016/j.spmi.2008.03.006
15. Fragalà ME, Malandrino G, Giangregorio MM, et al. Structural, Optical, and Electrical Characterization of ZnO and Al-doped ZnO Thin Films Deposited by MOCVD. Chemical Vapor Deposition. 2009; 15(10–12): 327–333. doi: 10.1002/cvde.200906790
16. Romero R, Leinen D, Dalchiele EA, et al. The effects of zinc acetate and zinc chloride precursors on the preferred crystalline orientation of ZnO and Al-doped ZnO thin films obtained by spray pyrolysis. Thin Solid Films. 2006; 515(4): 1942–1949. doi: 10.1016/j.tsf.2006.07.152
17. Islam MR, Rahman M, Farhad SFU, et al. Structural, optical and photocatalysis properties of sol–gel deposited Al-doped ZnO thin films. Surfaces and Interfaces. 2019; 16: 120–126. doi: 10.1016/j.surfin.2019.05.007
18. Badgujar AC, Yadav BS, Jha GK, et al. Room Temperature Sputtered Aluminum-Doped ZnO Thin Film Transparent Electrode for Application in Solar Cells and for Low-Band-Gap Optoelectronic Devices. ACS Omega. 2022; 7(16): 14203–14210. doi: 10.1021/acsomega.2c00830
19. Ilican S, Caglar M, Caglar Y. Determination of the thickness and optical constants of transparent indium-doped ZnO thin films by the envelope method. Materials Science-Poland. 2007; 25(3): 709-718.
20. Wu HW, Chu CH, Chen YF, et al. Study of AZO Thin Films Under Different Ar Flowand Sputtering Power by RF Sputtering. In: Proceedig of the International Multiconference of Engineers and Computer Scientists 2013; 13–15 March 2013; Hong Kong.
21. Born M, Oppenheimer R. Zur Quantentheorie der Molekeln. Annalen der Physik. 1927; 389(20): 457–484. doi: 10.1002/andp.19273892002
22. Hohenberg P, Kohn W. Inhomogeneous Electron Gas. Physical Review. 1964; 136(3B): B864–B871. doi: 10.1103/physrev.136.b864
23. Kohn W, Sham LJ. Vibrational frequency prediction using density functional theory Physical Review. 140(1965) 1133.
24. Kohn W, Sham LJ. Self-Consistent Equations Including Exchange and Correlation Effects. Physical Review. 1965; 140(4A): A1133–A1138. doi: 10.1103/physrev.140.a1133
25. Blaha P, Schwarz K, Sorantin P, Trickey SB. Full-potential, linearized augmented plane wave programs for crystalline systems. Computer Physics Communications. 1990; 59(2): 399–415. doi: 10.1016/0010-4655(90)90187-6
26. Blaha P, Schwarz K, Madsen G, et al. WIEN2k: An APW+lo program for calculating the properties of solids. The Journal of Chemical Physics. 2020; 7(152): 074101. doi: 10.1063/1.5143061